PAPER 82 – UNSTEADY PERFORMANCE OF DEGRADED COMPRESSOR AND TURBINE BLADES OF AN AERO-ENGINE AT VARYING AMBIENT AND TURBINE INLET TEMPERATURES

I.O. Otaiku[1], I. K. Adegun[2]

[1]International Aviation College, Ilorin, Kwara State and Kwara State University
[2]Department of Mechanical Engineering, University of Ilorin, Ilorin, Nigeria
Corresponding Author olaoluwaotaiku@yahoo.com. +23460520474.

ABSTRACT

The paper presents the modelling of unsteady performance of a degraded 4-stage compressor and single stage gas generator turbine blades of PT6T turboshaft aero-engine of a helicopter. The two sections were set as control volumes for analytical and numerical modeling. Numerically, The blade specimens (NACA 65 series) were developed using SOLIDWORKS 20 and simulations performed with FLUENT in ANSYS 20.0. The RANS (Reynolds-averaged Navier–Stokes) equations with Shear Stress Transport model SST (k-w) were chosen for the unsteadiness of pressure and temperature distributions over different levels of reductions in surface area of the blades' pressure side. 900 x 10^3 mesh elements size were selected and the boundary conditions-inlets for the two control volumes were 295-325 K and 1083 – 1245 K for compressor and turbine respectively. Analytically, equations for different levels of degradations (surface area reductions) were developed to determine their flow performance at new pressure and temperature for compressor and turbine with change in time and the corresponding rise in centrifugal stress. Results from FLUENT predicts the performance of the sections for 10% surface area reduction with complex structure in the turbulent flow imposes high fatigue stress, hence shows the highest closeness to surge margin. For the compressor, the result emphasizes the impact of inlet conditions on degraded blades over exit conditions. Also in the turbine, velocity contour shows adverse/backward flow as a result of high turbulence formation and rising fatigue due to change in exit pressure flow from stage to stage in the compressor. This exit pressure determines the TIT in the turbine which is a function of efficiency of the single stage gas generator turbine and is crucial to the overall efficiency of the engine and the safety of the engine as a whole. In conclusion, the inter-component flow behaviour between the degraded compressor and turbine as revealed in this study shows the near real-life situation of the engine performance. Summarily, the accurate engine life estimation can be deduced from TIT rising from 1100-1200 K and centrifugal stress 60MN/mm^2.

KEYWORDS: Specific fuel consumption (SFC), ambient temperature (ABT), turbine inlet temperature (TIT) and surface area degradation.

1. INTRODUCTION

1.1 The prediction of off-design steady and unsteady performance any gas turbine (industrial or aerospace) engines require the availability of compressor and turbine characteristics, which are pressure and temperature flow, pressure ratio and variation in their revolution per minute. Blades of the compressor and turbine sections operate at high temperatures and pressure depending on the materials they are made of and hence are capable to convert thermal energy into mechanical energy. During this process, the blades' mechanical properties are over-stretched beyond their design and manufacturing processes and therefore are bound to fail. This has been experimentally proven by the results presented by Otaiku and Adegun (2021). Failure of these blades while in operation have a negative impact on the engine performance and turbine efficiency. The aim and objective of this study is to model the performance of PT6T degraded engine and the impact of transient operations of a 4 stage compressor and single stage axial turbine under certain instance of changing temperatures at the compressor inlet/exit and the turbine inlet as the ambient pressure remains constant. Chernikov and Semakina (2023) used RANS SST model to predict the flow in a diffuser. Their results predicted 14% exhaust diffuser pressure recovery coefficient due to the complex vortex structure of the turbulent flow, which the ordinary Averaged Navier–Stokes equations could not resolve. The effect of compressor fouling/cracks and turbine wear have been evaluated by many scholars experimentally and numerically (Otaiku and

Adegun, 2021; Goeing, 2020; Srinival et al., 2018 and Xin et al., 2019) and approaches adopted in these literatures have used in this study with a better modified derived equations that were peculiar for the specimen developed. The work of Patel (2013); Vieweg, et al. (2019) and Kolias et al. (2021), categorically stated that levels of combined compressor and turbine wear were could be assumed to be a contributing factor for decrease in polytropic efficiency by 1% and 2% though there were no derivable methods to prove that these reductions in polytropic efficiencies were linked to a specific physical condition for the compressor or turbine. They also suggested that further study was required to correlate component efficiency and physical state which is the reason for this study and the gap has been covered going by the results presented.

1.2 Literature Review

Goeing (2020); Srinival et al. (2018); Xin et al. (2019) explained that the effect of compression ratio on compressor work is similar to turbine work. Change of air pressure from one flight level to the other, causes the work done by the compressor to change with the change in density As the work increased with increase in the compression ratio, it was expected that the ambient temperature also increased (Rahman et al., 2011).. A low ambient temperature produced high air density and a high gas turbine compressor work and output power. Increased tip clearances and changes in airfoil geometry will lead to unrecoverable condition of the section affected at these stated conditions. However, for the degraded blades the performance of the engine with variation in ambient temperature as a function of compressor work output affected the thermal efficiency of the engine as shown by Bayona-Roa et al. (2019); Liu et al. (2021) and Egorov et al. (2018). This was because, the air mass flow rate inlet to compressor increased with decrease of the ambient temperature. At 90% design speed, the losses in efficiency and pressure ratio were high due to fractured area of the blade pressure surface. It was also noticed that there was a reduction in efficiency of 22% as compared to that of on design configuration. Several researches carried out by Chernikov and Semakina (2023); Puspitasari et al. (2021) ; Deng et al. (2020); Srinivas et al. (2018); Klimko (2017); Rahman et al. (2011); Saravanamutto et al. (2009) and Camporeale et al. (2006) have clearly brought out that the margin to surge in the compressor stage was any speed less than 80-85% of the design speed. At this instance, the net power obtained form the difference between the turbine and compressor could make the shaft accelerate and move the operation point of the
compressor on the compressor map to a new position. In principle, surging is when the airflow through the whole compressor is stopped; stall effect is when only some stages are affected by flow break up. For this reason, the oscillation due to stalling can damage the compressor since it creates stress on the blades.

2. THEORETICAL ANALYSIS

The governing equations are derived by application of mass, momentum and energy equations. The unsteady Reynolds Averaged Navier Stokes (RANS) equation 1D model of fluid flow was used as a background. The dynamic effects such as the mass flow and work imbalances during engine transients were evaluated using the inter-component volumes method described in Fawke and Saravanamuttoo (1971). These transient operations existed in both compressor and high-pressure turbine. The numerical approach for modelling the unsteady performance of compressor-turbine in this study was as cited from Mathworks (2016); Camilo et al. (2019) and ANSYS Academic research (2016 and 2018) and represented as shown in Equations 1-10.:

2.1 Continuity Equation

$$\frac{\partial U_i}{\partial x_i} = 0. \quad (1)$$

$$\frac{\partial \rho}{\partial t} + \frac{\partial (\rho U_i)}{\partial x_i} = 0 \quad (2)$$

2.2 Momentum Equation

$$\frac{\partial (\rho u_i)}{\partial t} + \frac{\partial}{\partial x_j}\left(\rho u_i u_j\right) = \frac{\partial p}{\partial x_i} + \frac{\partial}{\partial x_i}\left[\, 2\mu s_{ij}\right] + \rho g_i + F_x \quad (3)$$

From Continuity Equation 3. The strain-rate tensor S_{ij} is given in Equation

$$S_{ij} = {}^{1}\!/_{2}\left(\frac{\partial (u_i)}{\partial x_j} + \frac{\partial u_j}{\partial x_i}\right) \quad (4)$$

Reynolds Averaged Thermal Energy Equation

$$\frac{\partial T}{\partial t} + \frac{\partial (u_i T)}{\partial x_i} = \frac{\partial}{\partial x_i}\left(\alpha \frac{\partial T}{\partial x_i}\right) + S \quad (5)$$

Reynolds averaged transport equation

$$\frac{\partial(\rho\Phi)}{\partial t}+\frac{\partial}{\partial x_j}(\overline{\rho u_i\Phi})=\frac{\partial}{\partial x_i}\left[\Gamma\left(\frac{\partial\Phi}{\partial x_i}-\overline{\rho u_i\emptyset}\right)\right]+\overline{S_p\Phi}+\overline{S_c} \quad 6$$

Reynolds time average Momentum or Navier-Stokes Equation (RANS)

$$\frac{\partial(\rho U_i)}{\partial t}+\frac{\partial}{\partial x_j}\left(\rho U_iU_j\right)=\frac{\partial P}{\partial x_i}+\frac{\partial}{\partial x_i}\left[\mu\overline{S_{ij}}\right]-\frac{\partial}{\partial x_j}\overline{\left(\rho U_iU_j\right)}+\tau_{ij} \quad 7$$

Where Reynolds stresses $\tau_{ij}=\overline{(\rho U_iU_j)}$

Transient Term

$$\rho\frac{\partial(\overline{U_i+u_i})}{\partial t}=\rho\frac{\partial U_i}{\partial t} \quad 8$$

Convective Term

$$\rho\frac{\partial[(\overline{U_i+u_i})(\overline{U_j+u_j})]}{\partial x_j}=\rho\frac{\partial[(\overline{U_iU_j+U_ju_i})(\overline{U_jU_i+U_iu_j})]}{\partial x_j} \quad 9$$

Pressure Term

$$\frac{\partial}{\partial x_i}(\overline{P+p})=\frac{\partial P}{\partial x_i} \quad 10$$

Assuming convective, pressure and viscous terms in above equations represent time averaged components and are equal to zero.

3. METHODOLOGY

Assumptions

In this study, the following assumptions were applied before developing equations.

a. Surface reductions changes with the blade length only as width remains constant.
b. The air/gas in both sections are compressible.
c. The equations were valid for laws of conservations.
d. The compression and turbine are adiabatic and isothermal.
e. The average heat flow to the surroundings is $\dot{Q}$.
f. The stagnation temperature is constant.

3.1 Problem formulation

Compressor and turbine blades experience repeated mechanical loadings during operation due to the large centrifugal stress caused by high rotational speed and temperature. Numerical and analytical methods were applied in this study to determine the rate of change of rotational speed at high temperatures to determine the quantity of fatigue (centrifugal stress) in the engine that will cause the reduction in the blade length and surface area.

3.2 Numerical Solution

The geometry of the blades and temperature range considered in this simulation were obtained from the experimental investigations carried out by Otaiku & Adegun (2021). In this numerical method, the blades were developed using SOLIDWORKS 20. Numerical solutions were obtained using ANSYS Fluent 20. The meshes were created in Mechanical APDL with 900×10^3 elements as the densest as shown in Figure 1a & b The boundary conditions for the compressor was set as 295 to 325 K and 1083 to 1235 K for the turbine. P_2, P_1 and P_4, P_3 represent the static pressures at the outlet and inlet of the compressor and turbine respectively. The simulation was performed in RANS $k-\omega$ Shear Stress Transport SST. This tool helps in running turbulent flow and facilitates the modelling of small element sizes (900×10^3 elements) that are smaller than the selected grid spacing. The time step was 0.001s. For each unsteady performance, over 500 iterations were executed to obtain results. The fluid was assumed as compressible air for compressor and gas for turbine. The turbulent flows depict fluctuating fluid velocity which can be characterized as high frequency in momentum and energy equations.

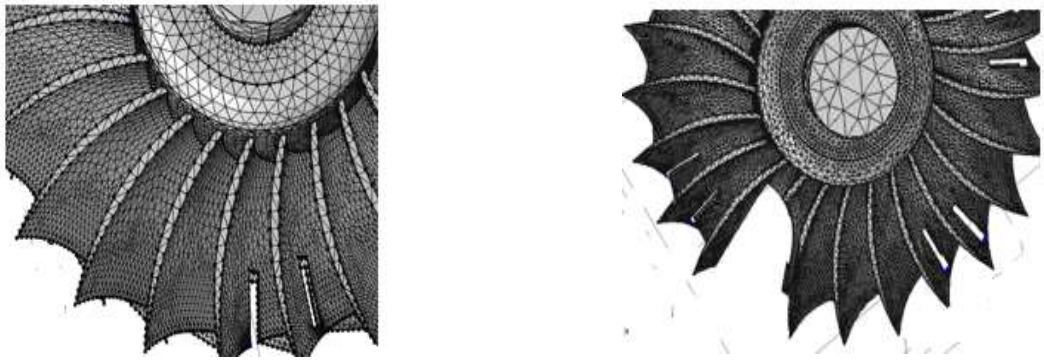

a. Formation of crack aize. b. 10% fractured area

Figure 1: Mesh specimen/

3.3 Analytical Method

The unsteady state for the compressor and turbine cause changes in mass flow rate, temperature and pressure rise. Figure 2 shows the position of the blades to the main engine discs which is used to derive the equations based on the assumptions (a-f).

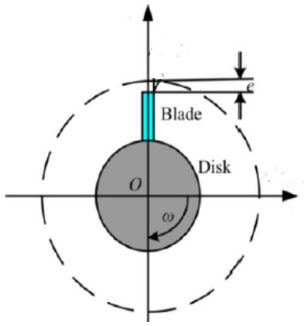

Figure 2: Blade on the compressor/turbine disk.

From Figure 2, the equation for percentage reduction in surface area can be obtained as given in Equation 11-12 below where initial radius at the tip

$$r_0^i = \frac{1}{2} l_0(t) + r_0(t) \quad (11)$$

radius at the root $r_h = r_0(t)$

New radius at the tip

$$r_{new}^i = \pi \left(\frac{1}{2} \overline{l}_{new} + r_0 \right)^2 \quad (12)$$

The characteristics of the flow was obtained by applying the energy balance in the control volume from Mark and Selwyn (2016) and Equations 1-3 with Equations 11-12 to derive the mechanical characteristics of the rotating blades as shown in Equations 13-22. For rotational transient conditions in x- direction, mass flow rate is as given in Equations 13 a and b.

Mass flow rate

$$\dot{m}_a = \rho v_a^i \pi \left[(r_{new}^i)^2 - \left(r_0^i \right)^2 \right] \quad (13a)$$

$$\dot{m}_{in} = \dot{m}_{out} = \rho \, V_{a1} \pi \left(\frac{1}{2} l + (r_{new}^i) \right)^2 = \rho V_{a2} \pi \left(\frac{1}{2} l + r_0^i \right)^2 \quad (13b)$$

Pressure per Stage

$$p^i = PR_s{}^i p^{i-1} \quad (14)$$

Temperature per Stage

$$T^i = \frac{\omega_c \eta^i M^i}{c_p \dot{m}_a} + T_0{}^{i+1} \quad 15$$

The stage pressure ratio P*R* is given by the following expression in Equation 16 by Varga et al. (2016) and using the derived mass flow rate in :

$$PR_s = \left[1 + \eta_s \frac{UC_a}{c_p T_{01}} (tan\beta_1 - tan\beta_2)\right]^{\frac{\gamma}{\gamma-1}} \quad 16$$

The temperature at the turbine exit is calculated by substituting temperature in Equation 15 into Equation 17 where the terms $\eta_{is,T}$and PR_Trepresents turbine efficiency and turbine pressure ratio respectively:

$$T_{out} = T_{in}\left[1 - \eta_{is,T}\left(PR_T{}^{\frac{\gamma-1}{\gamma}} - 1\right)\right] \quad 17$$

The PR_{Tc} for transient states in compressor and turbine is obtained using Equations 13 a and b derived for mass flow rate.

Torque

$$M^i = r^i \dot{m}_a (v_a^i)(tan\beta_1^i - tan\beta_2^i) \quad 17$$

Power

$$M^i \omega_c = \left[r^i \dot{m}_a (v_a^i)(tan\beta_1^i - tan\beta_2^i)\right]\omega_c \quad 18$$

3.4 Centrifugal Stress per Stage

The blade tip speed U will be limited by stress considerations at the root. With the assumption (a), the radius of the blade is constant at root r_h, then the equation for the centrifugal stress per stage at the root for varying blade length at the tip is obtained by modifying Equation 18 from Jim and Wesley (2019) as shown below:

$$\sigma_r = \int_{r_t}^{r_h} \rho_b \omega^2 r dr = 0.5\rho_b U_t^2 \left[1 - \left(\frac{r_h}{r_t}\right)^2\right] \quad 18$$

$$\sigma_C = \frac{F_c}{A_h} = \int_{r_h}^{r_t} \rho\, \omega^2 \frac{A_t}{A_h}\, rdr \quad 19$$

3.5 Centrifugal Stress with Rotational Speed

Following Equations 18 and 19, the centrifugal stress and changing surface area of the blade due to fracture or breakaway with rotational speed during the unsteady condition can be obtained by modifying equations developed from Krishnan et al., (2020); Sabila (2020); Alqallaf and Teixeira (2021) as shown in Equations 20 and 21.

$$AN^2 = \frac{360\sigma_t}{\pi\left(1+\frac{A_t}{A_h}\right)\rho_{blade}} \quad 20$$

$$\sigma_C = \frac{\rho\omega^2\left(\frac{1}{2}l+r\right)^2}{\pi}\left[2 - \frac{2}{3}\left(1 - \frac{A_h}{A_h}\right)\left(1 + \frac{1}{1+\frac{r_h}{r_t}}\right)\right] \quad 21$$

So that new length according to degradation (Figure 3) level are

$$l = 17.04\ mm\ (0\%), 14.87\ mm\ (8\%)\ \&\ 14.5\ mm\ (10\%)$$

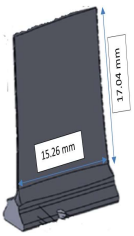

Figure 3: Present Specimen

4. RESULTS AND DISCUSSION

4.1 Increase in Pressure and Temperature

Figures 4, 5 and 6 show profile of the pressure at the 4- stage compressor and the single stage gas generator turbine for 0% degradation. The pressure contours for the two sections were similar to those predicted by Hocko (2019) as shown in Figure 7. Here, for each increase in the compressor exit temperature and TIT for the turbine, changing inlet parameters would not significantly affect the performance when on on-design parameters or according to manufacturer's specifications as shown in Figure 4 and 6. . However, during transient conditions with increment of time change, ambient parameters significantly affect exit pressure and temperature depending on the level of degradation as shown in Figures 8 and 9. However, the results obtained in the experiment were similar to those predicted by RANS in the simulation. The difference between them was because the experimental data were obtained from static position. Comparing the numerical results with previously obtained experimental results, it can be said that the effect of astronomical increase in pressure flow of hot air and gas is due to presence of cracks by extension, dislocations and disorientations of the densely packed grains of the blades constituent elements which could eventually result into heavy material loss.

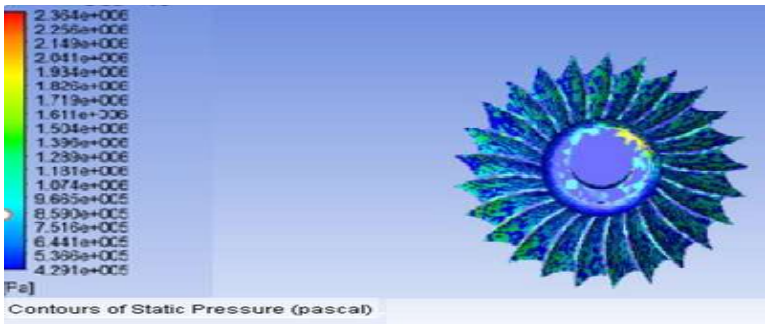

Figure 4: Undegraded (0%) compressor blades.

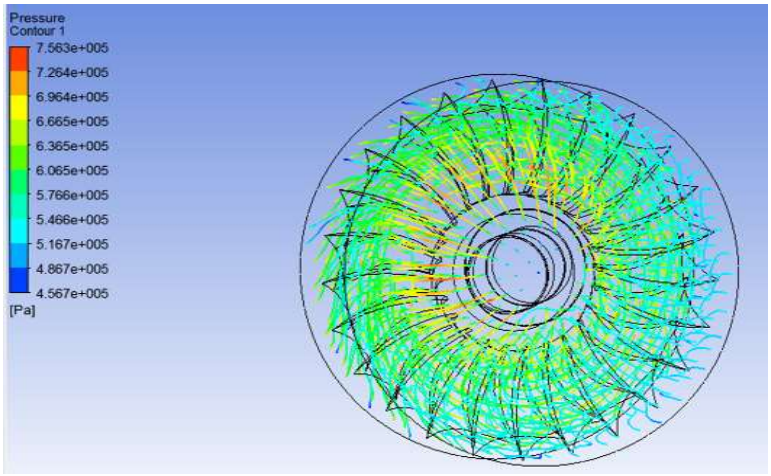

Figure 5: Undegraded (0% degradation) Turbine blades.

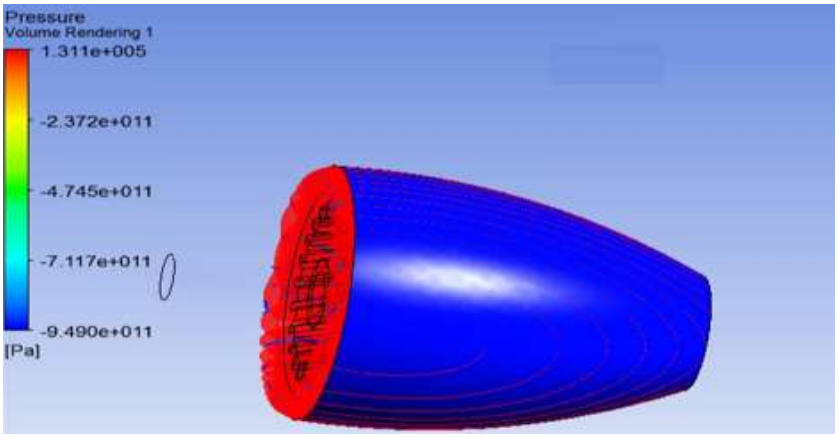

Figure 6: Evenly distributed pressure flow-
Turbine assembly.

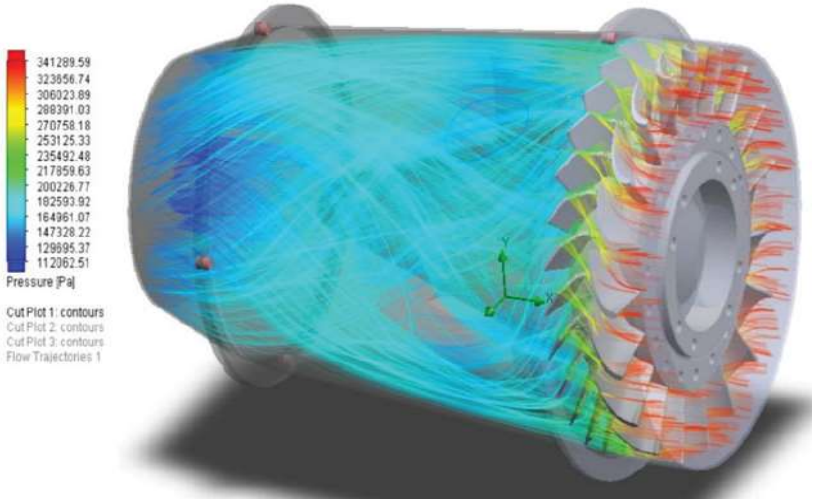

Figure 7: Pressure flow from tip to hub
Source: Hocko (2019).

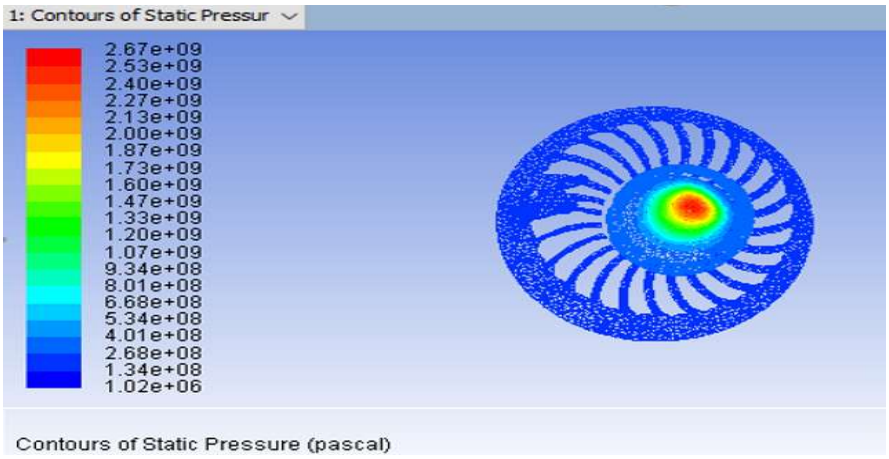

Figure 8: 8% degradation blades

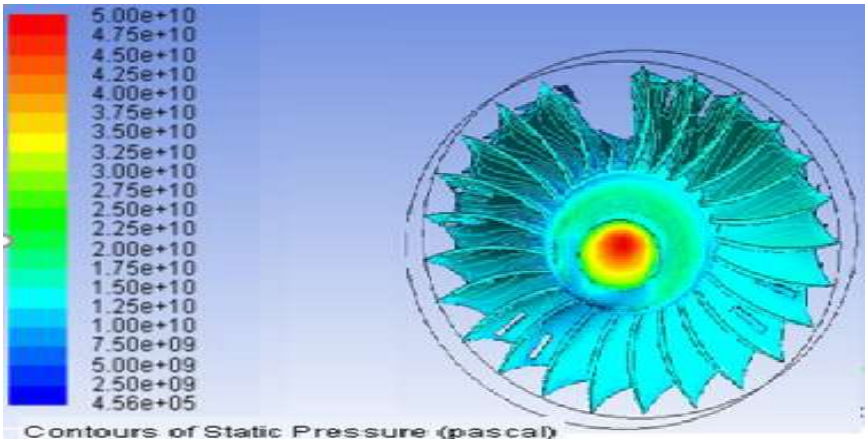

Figure 9:10% degradation.

4.2 Temperature Contour

In the same sense like pressure, temperature contours for the compressor and the turbine for steady state is as shown in Figures 10 and 11 with the ambient conditions applied.

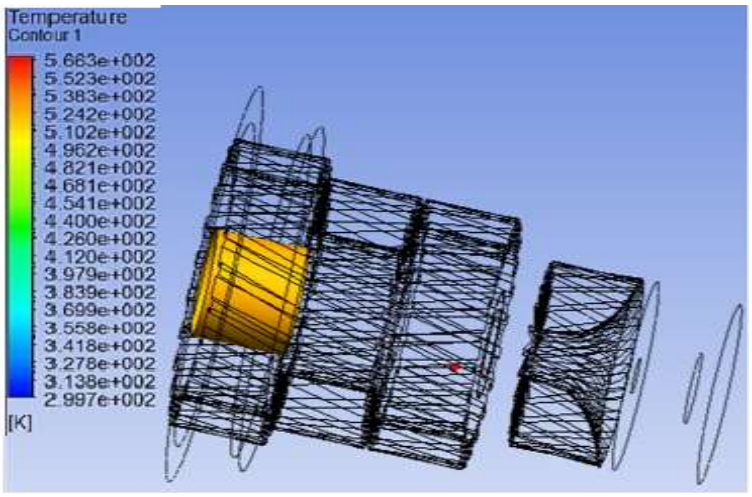

Figure 10: Effect of ambient temperature on compressor exit temperature (4- stage compressor assembly).

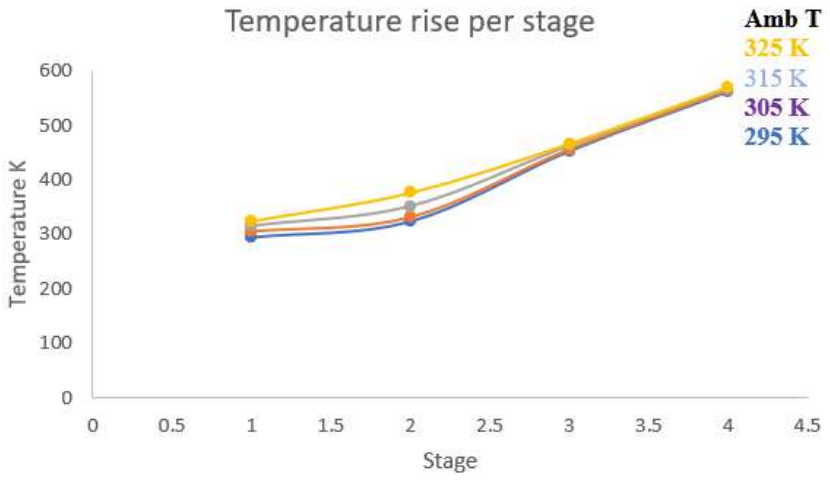

Figure 11: Insignificant effects of ambient temperature on compressor exit temperature.

Here ambient temperatures T1 in the range of 295 to 325 K were producing constant compressor exit temperatures T2 with little or no variations as shown in Figure 11. After the initial changes in pressure and temperature parameters, RANS model selected in FLUENT gave a convincing result of the new state of the sections being studied as shown in Figures 12-15.

In furtherance to the investigation of blades degradations, Figure 12 show the turbine inlet temperatures increasing beyond allowable value as shown.

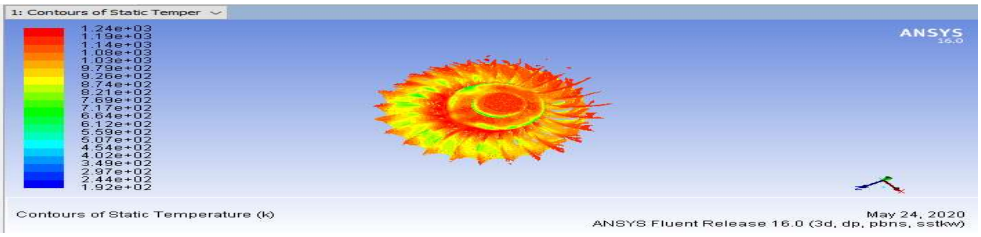

Figure 12: Too high Turbine Inlet Temperature.

This increase in TIT (T3) is precipitated by sudden increase in temperature T2 from the compressor depending on the level of degradation as analytical solutions show in Figures 13 and 14.

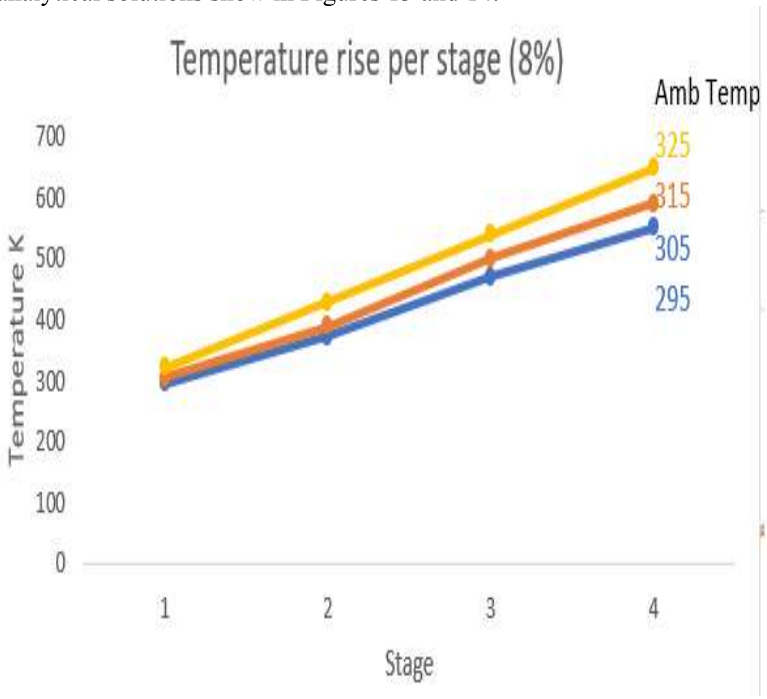

Figure 13: 8% degradation (4-compressor)

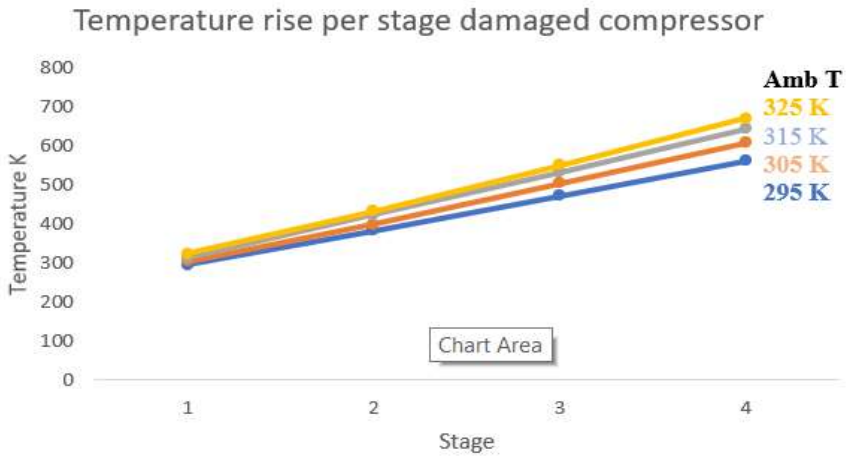

Figure 14: 10% degradation (4-stage compressor).

As can be seen from Figure 14, ambient temperature of 315 K produced analytical value of ≈ 570 K as compressor exit temperature for an 8% surface area degradation. Increase in temeprature beyond this level of degradation will severely affect the compressor exit temperature as compared to simulation result obtained in Figure 15 showing ≈ 569 K at the same ambient temperature. At 325 K, compressor exit temperature for 8 and 10% blade degradation will astronomically increase beyond the permisssible working temperature of the Ti-6AL-4V material of the blades in the compressor. Figure 15 show already degraded cowling and deformed outer surface of the compressor assembly due to this astronomical exit temperature and will continue to increase as long as the ambinet temperature increases and worsen the condition of the blades and the engine at large. This simulated or analytical temperature value will berth the badly damaged turbine condition as shown in Figures 12 and 16 respectively.

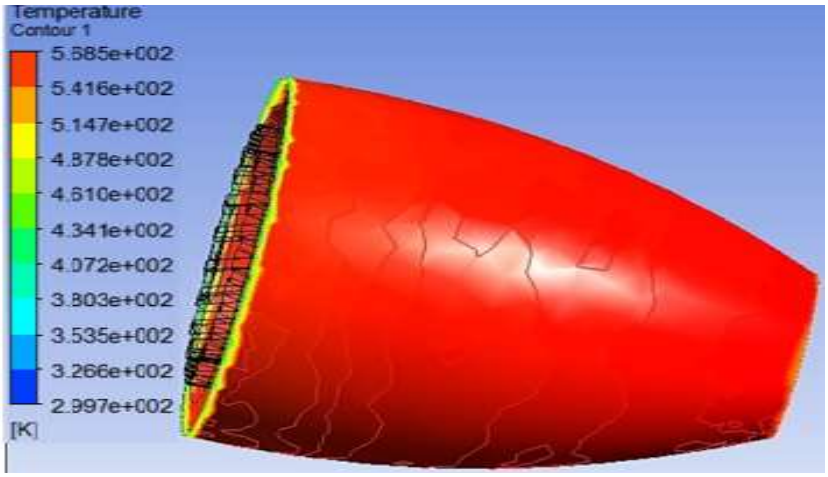

Figure 15: Effect of change in ambient temperature on compressor exit temperature for 10% degradation.

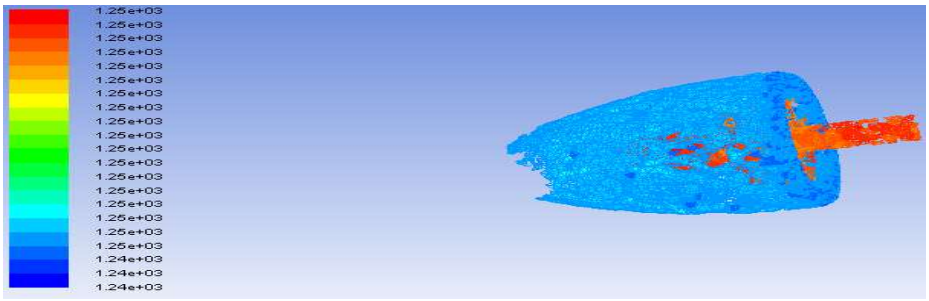

Figure 16: 10% degradation in the turbine

4.3 Velocity Contour

The mean velocity contour obtained from the unsteady simulation showed (Figure 17) high turbulent swirl and reversal flow especially in the turbine to depict the level of degradation of turbine and its closeness to approaching surge margin at temperatures beyond 315 K. This condition will aggravate as the engine shaft speed in RPM increases.

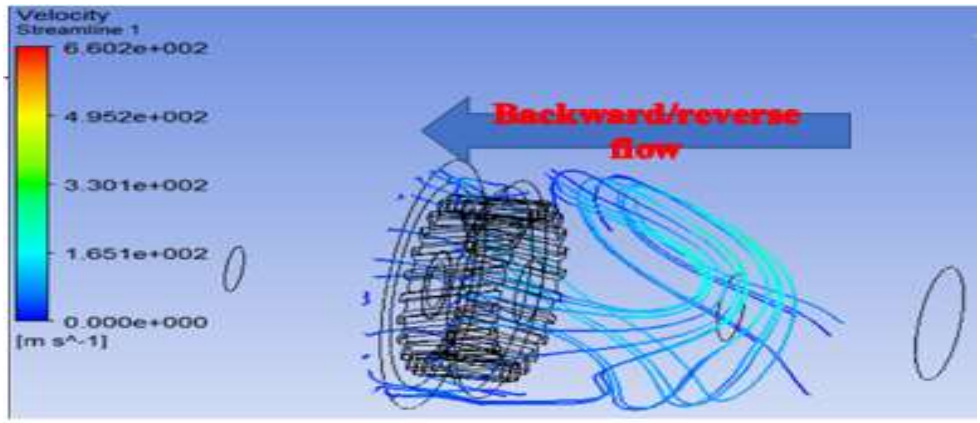

Figure 17: Flow reversal and turbulence flow in the turbine with 10% degradation.

As stated earlier, the velocity contour at the turbine shows large reversal flow due to 10% surface area reduction of the blades in the turbine enclosure.

4.3 Centrifugal stress

Centrifugal stress values for 0-10% surface area degradation was analytically obtained as shown in Figure 18. As can be viewed from Figure 17, flow reversal in the turbine and high rotating speed of the turbine shaft will impose high risk centrifugal stresses on the blades. At instances of high ambient and compressor exit temperatures the compressor and the turbine will experience near rotating stall otherwise known as surge condition reason for the need to check ambient and turbine inlet temperature when blade degradation is noticed. Flying in warm air ISA condition for degraded engine is a recipe for unsafe flight.

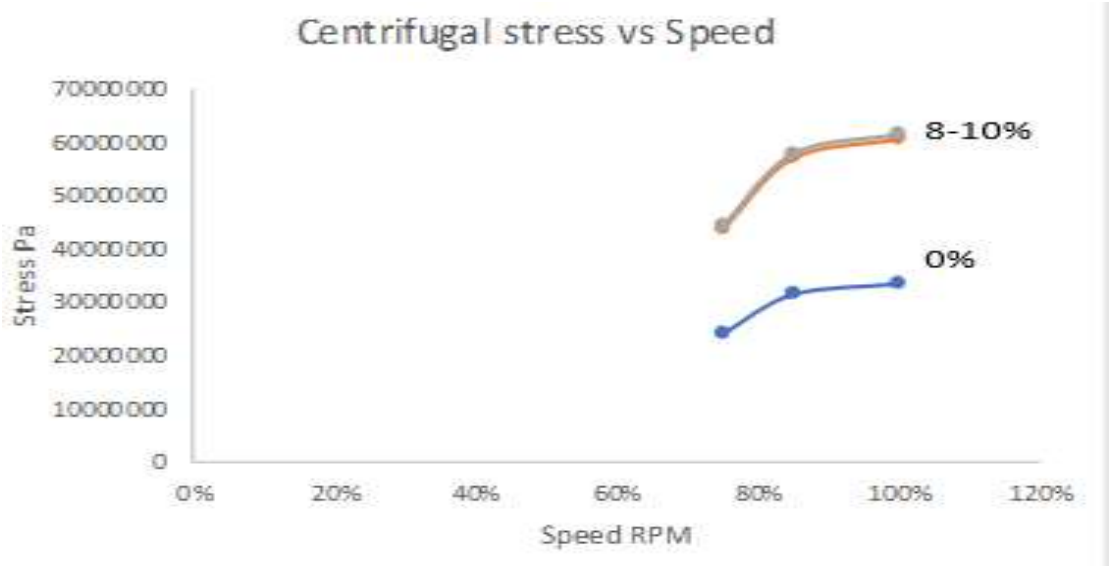

Figure 18: Centrifugal stress versus degradation level.

5. CONCLUSION

The operating pressure and temperature are important performance parameters in the compressor and turbine of gas turbine engines. So for a steady flow performance, on design parameters at the outlet of the compressor and the inlet of the turbine must be as specified. However, in real life operations, these parameters are sometime exceeded above the permissible range of the materials for the stage or section. Analytical and simulations results conducted in this study showed that astronomical increase above specified pressure and temperature ranges would cause degradations of the blades leading to severe unsteady performance. Once degraded, higher inlet/ambient temperature into the compressor would produce higher exit and inlet temperatures at the compressor and turbine respectively. Degradation from 0 -10% were simulated and analysed as 10% and above was found worse off above 315 K (ambient temperature) which could lead to permanent engine failure. Any change above 315 K for such level of degradation would cause flow reversal in the turbine due to higher TIT and could lead to a rotating stall or surge. Centrifugal stress (60 kN/m^2) imposed on the blades during the new condition would cause engine burn-out which is hazardous to safety during flight.

6. Recommendations

In the event of stall before surge during flight operations, the maximum engine RPM should not exceed 80% and at TIT above 1092 K. On this note, Engine Manufacturers are advised based on this study to incorporate Centrifugal Stress Engine Instrument that will indicate the centrifugal stress levels of the engine at any face of flight to make on spot decision by the crew to mitigate against risk of more fractured blades and breakaways which is hazardous to flight safety. For further study, experiment should be carried out on rotating blades of the compressor and the turbine.

7. APPENDICE

7.1 Euler Tubomachinery Equation

The Euler turbine equations for work in terms of wheel speed, relative velocity, and absolute velocity are given in this section in Equations 22-25. As the turbine produces more power than is required to drive the compressor during transient condition, the shaft accelerates until a new balance point between the compressor and turbine power is found. It is vice versa, for the compressor so that as it uses more power than the turbine is able to deliver, deceleration of the shaft occurs. The difference between the turbine and the compressor, i.e the surplus power, is obtained from Equation 22:

$$SP = \eta_m \dot{m}_2(h_3 - h_4) - \dot{m}_1(h_2 - h_1) \quad (22)$$

7.2 Surplus Power of the Dynamic Turbine Shaft

Inertia of the shaft consisting the turbine and compressors axes against any change in shaft rotational speed as a function of shaft power is as shown in Equation 23 – 24.

$$SP = M\omega = I\alpha\,(2\pi N) = I\frac{d\omega}{dt}\,2\pi N = \frac{4\pi^2\, I\, NdN}{dt} \quad (23)$$

7.3 Dynamic Rotational Speed

Theoretically, the new rotational speed for a change in power (surplus power) is as given in Equation 24-26

$$\frac{dN}{dt} = \frac{SP}{4\pi^2\, I\, NdN} \quad (24)$$

Numerically, this is solved using Equation 25

$$N = \int_t^{t+dt} \frac{SP}{4\pi^2\, I\, NdN} \quad (25)$$

Otherwise using Euler Equation, the dynamic rotational speed is as given in Equation 26:

$$N_{new} = N_{old} + \left(\frac{dN}{dt}\right)_{new}.\Delta t \quad (26)$$

8. ACKNOWLEDGEMENT

The authors would like to thank University of Ilorin especially Profs, AGF Alabi, Aweda and Alao for their advisory role. Also worthy of note is Tgt. Rasheed from Kwara State for providing laboratory facilities for the simulation and

experimental results respectively. Also, very special thanks to Petroleum Technological Development Fund (PTDF) for the financial support for my Ph.D work and Police Air Wing Abuja (ACP Ndubuisi and Engr. Cosmos Eze).

9. Conflict of Interest

The authors declare that no conflicting interest.

10. Data Availability

Operating data from the Aircraft Maintenance Manual from the manufacturer was used.

11. REFERENCES

Otaiku I.O and Adegun I.K. (2021). Investigation of preliminary factor leading to first-third stage blade cracks initiation, growth and their effects on aero-engine performance. The Nigerian Institute of Mechanical Engineers, 34th International Conference and Annual General Meeting (2021).

Marek Klimko (2017) "Strength analysis of an aircraft turbo-compressor engine turbine disc, Cite as: AIP Conference Proceedings 1889, 020019 (2017); https://doi.org/10.1063/1.5004353.

Saravanamutto, H. I. H; Rogers, G. F.C., Cohen, H., Strazincky P. V., (2009): Gas Turbine Theory, 6th ed., Pearson Education Limited, ISBN: 978-0-13-222437-6, 2009

Rahman M. M., Ibrahim T.K, and Abdalla A.N, (2011). Thermodynamic performance analysis of gas-turbine power-plant. International Journal of the Physical Sciences Vol. 6(14), pp. 3539-3550, 18 July, 2011 http://www.academicjournals.org/IJPS

DOI: 10.5897/IJPS11.272. ISSN 1992 - 1950 ©2011 Academic Journals

Deng C., Abdalla A.N., Ibrahim T.K., Jiang M.X., Al-Sammarraie A.T., and Wu J. (2020). Implementation of Adaptive Neuro-fuzzy Model to Optimize Operational Process of Multiconfiguration Gas-Turbines. Advances in High Energy Physics Volume 2020, Article ID 6590138, 17 pages. https://doi.org/10.1155/2020/6590138

Camporeale, S. M.; Fortunato, B.; Mastrovito, M. A (2006). Modular Code for Real Time Dynamic Simulation of Gas

Turbine in Simulink. Transactions of the ASME, v. 128, p. 506-517, July 2006.

Srinivas G., Raghunandana K., and Satish S.B. (2018) Axial-flow compressor analysis under distorted phenomena at transonic flow conditions, Cogent Engineering, 5:1, 1526458, DOI: 10.1080/23311916.2018.1526458

Puspitasari P., Andoko A., and Kurniawan P. (2021) Failure analysis of a gas turbine blade: A review. https://www.researchgate.net/publication/350161777 Failure analysis of a gas turbine blade: A review Article *in* IOP Conference Series Materials Science and Engineering · February 2021 DOI: 10.1088/1757-899X/1034/1/012156.

Yadav M., Misr A., Malhotra A. and Kumar N. (2019). "Design and analysis of a high-pressure turbine blade in a jet engine using advanced materials", *Materials Today: Proceedings [Internet]*. 2019 Aug 16 [cited 2019 Nov 22]; Available from: https://www.sciencedirect.com/science/article/pii/S2214785319327191.

Rao V.N.B., Kumar I.N.N., Prasad K.B., Madhulata N., Gurajarapu N. (2014), "Failure mechanisms in turbine blades of a gas turbine Engine –an overview", *Int. J. Eng. Res. Dev*, Vol. 10, pp.48-57, 2014.

Vasilyev, B.; Selivanov, A. (2019) Numerical method of single-crystal turbine blade static strength estimation taking into account plasticity and creep effects. Mater. Phys. Mech. 2019, 42, 311–322

Chernikov, V.; Semakina, E. (2023) Experimental and Numerical Studies of the Aerodynamics of Stationary Two-Shaft Gas Turbine Exhaust System. Energies 2023, 16, 3671. https://doi.org/10.3390/en16093671.

Kuschel, M.; and Seume, J.R. (2011). Influence of Unsteady Turbine Flow on the Performance of an Exhaust Diffuser. In Turbo Expo: Power for Land, Sea, and Air; Volume 7: Turbomachinery, Parts A, B, and C; ASMEDC: Houston, TX, USA, 2011; pp. 1551–1561.

Fleige, H.-U.; Riess, W.; Seume, J. (2002) Swirl and Tip Leakage Flow Interaction with Struts in Axial Diffusers. In Turbo Expo: Power for Land, Sea, and Air; Volume 5: Turbo Expo 2002, Parts A and B; ASMEDC: Houston, TX, USA, 2002; pp. 871–878.

Vasilyev B., Nikolaev S., Raevskiy M., Belov S. and Uzhinsky I. (2020) Residual Life Prediction of Gas-Engine Turbine Blades Based on Damage Surrogate-Assisted Modeling. Appl. Sci. 2020, 10, 8541; doi:10.3390/app10238541.

Janikovič J., Pilidis and Singh (2010) Gas Turbine Transient Performance Modeling for Engine Flight Path Cycle Analysis.

NOMENCLATURE

A = area (m2)
Alt = altitude (m)
C = speed of sound (m/s)
Va = velocity of air at inlet (m/s)
Cp = specific heat at constant pressure (kJ/kgK)
F = thrust
FAR= fuel air ratio
h = specific enthalpy (kJ/kg)
LHV=lower heating value of fuel (kJ/kgK)
m = mass flow rate of fluid (kg/s)
*m*a = mass flow rate of air at inlet (kg/s)
*m*f = fuel mass flow rate (kg/s)
M = Mach number
p = total pressure (bar)
ps = static pressure (bar)
RpC = compressor pressure ratio (overall)
R = characteristic gas constant
s = specific entropy (kJ/kgK)
SFC= specific fuel consumption (kg/Nh)
T = total temperature (K)
Ts = static temperature (K)
TIT = turbine inlet temperature (K)
W = specific work (kJ/kg)

Greek Symbols

Δp = pressure loss
γ = specific heat ratio
ρ = density
η = efficiency (%)

Suffixes

a = air
amb = ambient
b = burner
g = gas
p = pressure